ACTUATORS

Hexagonal electrohydraulic modules for rapidly reconfigurable high-speed robots

Zachary Yoder[1,2]†, Ellen H. Rumley[1,2]†, Ingemar Schmidt[1], Philipp Rothemund[3], Christoph Keplinger[1,2,4]*

Copyright © 2024 The Authors, some rights reserved; exclusive licensee American Association for the Advancement of Science. No claim to original U.S. Government Works

Robots made from reconfigurable modular units feature versatility, cost efficiency, and improved sustainability compared with fixed designs. Reconfigurable modules driven by soft actuators provide adaptable actuation, safe interaction, and wide design freedom, but existing soft modules would benefit from high-speed and high-strain actuation, as well as driving methods well-suited to untethered operation. Here, we introduce a class of electrically actuated robotic modules that provide high-speed (a peak contractile strain rate of 4618% per second, 15.8-hertz bandwidth, and a peak specific power of 122 watts per kilogram), high-strain (49% contraction) actuation and that use magnets for reversible mechanical and electrical connections between neighboring modules, thereby serving as building blocks for rapidly reconfigurable and highly agile robotic systems. The actuation performance of each hexagonal electrohydraulic (HEXEL) module is enabled by a synergistic combination of soft and rigid components; a hexagonal exoskeleton of rigid plates amplifies the motion produced by soft electrohydraulic actuators and provides a mechanical structure and connection platform for reconfigurable robots composed of many modules. We characterize the actuation performance of individual HEXEL modules, present a model that captures their quasi-static force-stroke behavior, and demonstrate both a high-jumping and a fast pipe-crawling robot. Using embedded magnetic connections, we arranged multiple modules into reconfigurable robots with diverse functionality, including a high-stroke muscle, a multimodal active array, a table-top active platform, and a fast-rolling robot. We further leveraged the magnetic connections for hosting untethered, snap-on driving electronics, together highlighting the promise of HEXEL modules for creating rapidly reconfigurable high-speed robots.

INTRODUCTION

Modern robots excel at executing specialized tasks in structured environments. It remains a challenge, however, to develop robots with sufficient versatility for responding to unpredictable circumstances without incurring high computational and material costs (*1*, *2*). One promising approach for developing accessible and versatile systems is through robots that are composed of modular building blocks that can be arranged together and rapidly rearranged into different configurations, enabling the robot to meet evolving needs (*3*–*9*). In addition, reusing existing parts and swapping out locally damaged units save costs and promote a robust and sustainable design. Additional capabilities such as self-assembly and automated formation of various geometries using independently controllable units highlight the unique benefits offered by a modular approach (*10*–*17*). A common limitation of such designs, however, lies in their actuation components; the use of traditional dc motors, although they are capable of high forces and precise motion, restricts robots by contributing to their weight or by limiting possible form factors (*18*, *19*).

Conversely, soft actuators are inspired by natural muscle and use lightweight, conformal materials to enable robotic capabilities that are otherwise challenging to achieve with conventional driving components (*18*–*22*); existing soft actuators have successfully demonstrated wide adaptability (*23*), inherent safe interaction with surroundings (*24*, *25*), high energy efficiency (*26*, *27*), and resistance to mechanical damage (*28*–*30*).

However, robotic modules driven by soft actuators have yet to demonstrate the well-rounded blend of attributes necessary for agile, multifunction reconfigurable systems, namely, high-speed and high-strain actuation, driving methods well suited to untethered operation, and modular connection schemes that enable rapid and diverse reconfigurability. Pneumatic soft actuators have been effectively used in previous works to drive a variety of modules that enable reconfigurable robots with impressive capabilities (*31*–*37*); however, these modules require arrays of bulky valves that can make reconfiguration cumbersome, and pneumatic actuation generally necessitates heavy and inefficient air compressors that limit the actuation speed of the modules and the agility of the resulting robots. Shape memory alloys (SMAs) (*38*–*40*) and dielectric elastomer actuators (DEAs) (*41*–*46*) are electrically driven, and modules actuated by these technologies have elegant connection schemes and untethered operation. However, the heating and cooling processes that drive SMAs are relatively slow, and existing DEA modules show limited actuation strain and are composed of stretchable materials that present manufacturing challenges.

Soft electrostatic actuators that use solid-liquid dielectric architectures can achieve fast (*47*), highly versatile (*48*–*50*), electrically driven actuation (*51*, *52*) and can be made from flexible, nonstretchable materials with high dielectric strength that are compatible with readily available manufacturing methods (*53*–*59*). In particular, this class of soft actuators features wide design freedom and diverse actuation modes (*26*, *60*–*64*), making them attractive candidates to explore for use in modular and reconfigurable robots.

Here, we present a class of electrohydraulically driven robotic modules with high-speed (contractile strain rate of 4618%/s) and

[1]Robotic Materials Department, Max Planck Institute for Intelligent Systems, Stuttgart, Germany. [2]Paul M. Rady Department of Mechanical Engineering, University of Colorado, Boulder, CO, USA. [3]Institute for Adaptive Mechanical Systems, University of Stuttgart, Stuttgart, Germany. [4]Materials Science and Engineering Program, University of Colorado, Boulder, CO, USA.
*Corresponding author. Email: ck@is.mpg.de
†These authors contributed equally to this work.

Downloaded from https://www.science.org at Max Planck Society on September 23, 2024

high-strain actuation (49% contraction) that leverage a magnetic connection scheme for rapid and reversible mechanical and electrical connections between modules, enabling a variety of agile, reconfigurable robots that can be driven by untethered, snap-on driving electronics (Fig. 1 and Movie 1). The fast and large-stroke actuation capabilities of each hexagonal electrohydraulic (HEXEL) module are derived from a synergistic combination of soft and rigid components; a hexagonal exoskeleton of rigid plates serves a dual purpose of amplifying the shape change produced by soft electrohydraulic actuators and providing a mechanical structure for effectively translating forces and torques throughout larger, reconfigurable systems (Fig. 1, A to C). This approach enables versatile behavior, which we demonstrated by rearranging the same group of six HEXEL modules into a high-stroke muscle, a multimodal active array, a table-top active platform, and a fast-rolling robot (Fig. 1, D to G), allowing for modules to collectively display diverse actuation modes and robotic capabilities beyond what each module could accomplish alone.

RESULTS

Actuation principle

Our design architecture takes inspiration from the vast number of biological systems that use stiff materials, like bones and exoskeletons, to both modify the mechanical output of soft muscles and

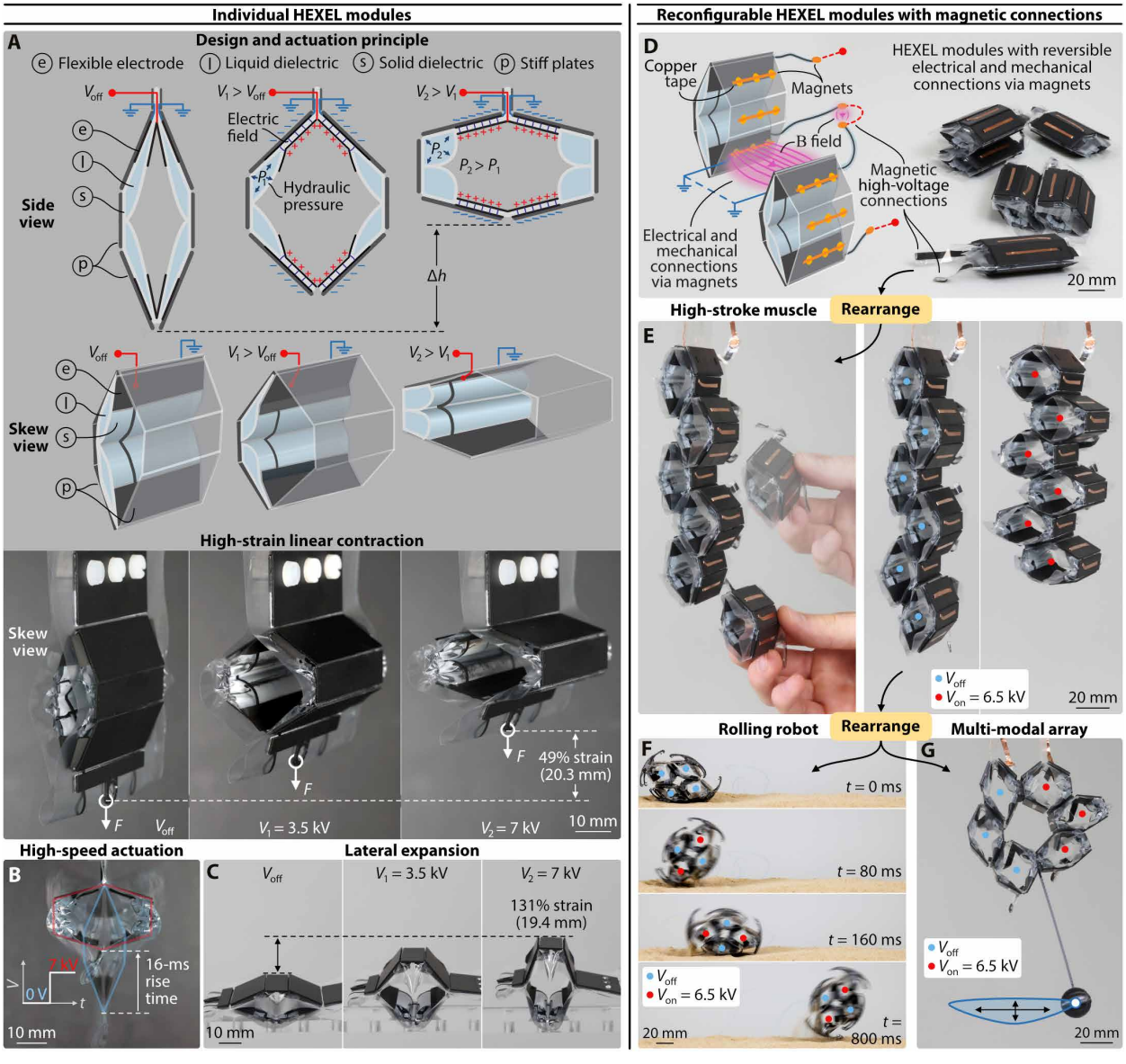

Fig. 1. HEXEL modules for reconfigurable robots. (**A**) HEXEL modules are composed of four soft electrohydraulic actuators integrated into a rigid hexagonal exoskeleton. The rigid plates amplify the shape change produced by the electrohydraulic actuators, resulting in controllable, high contractile strains and (**B**) high actuation speeds. (**C**) HEXEL modules also display controllable lateral expansion upon actuation. (**D**) Embedded magnets enable rapid, reversible mechanical and electrical connections between reconfigurable HEXEL modules. The B field refers to the magnetic fields between modules and between high-voltage leads. The same group of HEXEL modules was reconfigured into (**E**) a high-stroke muscle, (**F**) a rolling robot, and (**G**) a multimodal active array. The scale bars are 10 mm long in (A) to (C) and 20 mm long in (D) to (G).

Downloaded from https://www.science.org at Max Planck Society on September 23, 2024

Movie 1. Working principle and demonstrations of HEXEL modules. HEXEL modules produce high-speed, high-strain actuation and serve as building blocks in rapidly reconfigurable robots that can be driven by untethered, snap-on driving electronics.

provide a stiff structure that effectively translates forces and torques throughout the system. In this way, we used rigid plates to transform the shape change of soft electrohydraulic zipping actuators into rapid, large-stroke actuation. Inspired by previous work that leveraged a hexagonal, six-bar linkage for strain amplification (*65*), we situated actuators on the basis of hydraulically amplified self-healing electrostatic (HASEL) actuation technology (*53*, *54*) at the junctions of a hexagonal array of stiff plates. Applying a nonzero voltage V_1 across the electrodes of each actuator pouch induces a Maxwell stress that causes the electrodes to zip together and drives the liquid dielectric away from between them (Fig. 1A). This increases the hydraulic pressure in each pouch to P_1, resulting in pouch deformations (*54*) at the hexagon vertices. A greater voltage magnitude ($V_2 > V_1$) yields a greater Maxwell stress, further increasing the hydraulic pressure ($P_2 > P_1$) and resulting actuation until the electrodes are fully zipped together. This drives a fast shape change in the hexagonal cross-section of a HEXEL module (Fig. 1B and movie S1); a reference module linearly contracted (from 41.6 to 21.3 mm in length; Fig. 1A), and it simultaneously laterally expanded (from 14.7 to 34.1 mm in width; Fig. 1C).

Individual HEXEL modules are composed of inexpensive and widely available materials, including thermoplastic film, conductive carbon ink, tape, and fiberglass plates. The fabrication of HEXEL modules and the specific materials used are described in detail in Materials and Methods and Supplementary Materials and Methods (fig. S1).

High-speed and high-strain actuation

Linear contraction

We first analyzed the contractile dynamic response of a representative HEXEL module (Fig. 2) using a reference geometry, as defined in Materials and Methods. For reference actuation conditions, we applied a maximum electric field of 235 V/μm (correlating to a voltage of 7.05 kV for reference modules), which we experimentally determined as an upper limit for reliable yet high-performance actuation; higher electric fields improved performance but increased the likelihood of electrical breakdown (*66*).

In response to a square-wave driving signal, a reference HEXEL module reached a maximum of 49% free contractile strain (20.3-mm stroke), with a rise time of 16 ms and a fall time of 41 ms (Fig. 2A and movie S2). We further characterized the response of the module to a square-wave signal under various loads (Fig. 2, B and C). The HEXEL module exhibited a peak contractile strain rate of 4618%/s, which hyperbolically decreased with increasing load; nevertheless, at the highest tested load of 200 g, the HEXEL module maintained a peak strain rate of nearly 600%/s. We measured a peak specific power of 122 W/kg under a 100-g load, with a maximum average of 57 W/kg. The specific power of the HEXEL module was competitive with most reported mammalian muscles, and the peak strain rate of the module far exceeded that of muscle (*67*, *68*).

We next measured the stroke under no load when applying sine wave driving signals with amplitudes of 6 kV over a range of frequencies to determine the bandwidth of the module (Fig. 2, D and E, and movie S3). We used the stroke at low frequency (16.8 mm, measured at 0.5 Hz) to normalize the data and found a bandwidth of 15.8 Hz (Fig. 2E). The HEXEL module exhibited subharmonic actuation behavior in the frequency range of 17 to 25 Hz; in this range, the frequency of the actuation stroke was half of the frequency of the driving signal (for example, the module responded at 11 Hz when driven by a 22-Hz signal) (Fig. 2D, fig. S2, and movie S3). This phenomenon is observed in a variety of soft electrostatic actuators, including DEAs and spider-inspired electrohydraulic soft-actuated (SES) joints (*26*, *69*, *70*). For actuation frequencies of 6 to 9 Hz and 18 to 19 Hz, the module displayed an out-of-plane instability (movie S3). Such resonance behavior may introduce challenges when controlling robotic devices, although this issue would likely be eliminated if the robotic component controlled by the module had larger mechanical inertia than the module itself.

Lateral expansion

We also characterized the square-wave response of a HEXEL module in the secondary, lateral expansion actuation mode (fig. S3). This revealed a rise and fall time of 15 and 40 ms, respectively, with a maximum strain of 113% (fig. S3A) and a peak strain rate of 11,204%/s (fig. S3B), a peak specific power of 90 W/kg under a 30-g load, and a maximum average specific power of 33 W/kg (fig. S3C).

Modeling quasi-static force-stroke behavior

To understand the influence of various design parameters on actuation performance, we developed and validated a model that predicts the quasi-static, contractile force-stroke curves of HEXEL modules (Fig. 3). This modeling approach builds on previous models developed for Peano- and planar-HASEL actuators (*71*–*73*), as well as SES joints (*26*).

Each HEXEL module was made up of a regular arrangement of four pouches constrained with stiff plates (Fig. 3A). To simplify our modeling approach, we assumed both horizontal and vertical symmetry across the module. Thus, we could calculate the shape of the entire HEXEL module from the analysis of one quadrant.

For each quadrant, we analyzed three geometric states: unfilled, filled with liquid dielectric, and actuated (Fig. 3A). The unfilled state consisted of two vertically oriented plates. Plate 1 had a length of $L_1 + L_3$, and plate 2 had a length of L_2. Adhered to the plates was a pouch with electrode length L_e and electrode-free length L_n. In the filled state, the pouch contained an incompressible liquid dielectric with volume v. The pouch had a cross-sectional area $A = \frac{v}{w}$ (where w is the pouch width), causing the bending angle θ to become nonzero. Because of the assumed symmetry, plate 2 always remained vertical, and both joints rotated by the same angle θ. When a voltage was applied to the electrodes, a Maxwell stress was generated across

Downloaded from https://www.science.org at Max Planck Society on September 23, 2024

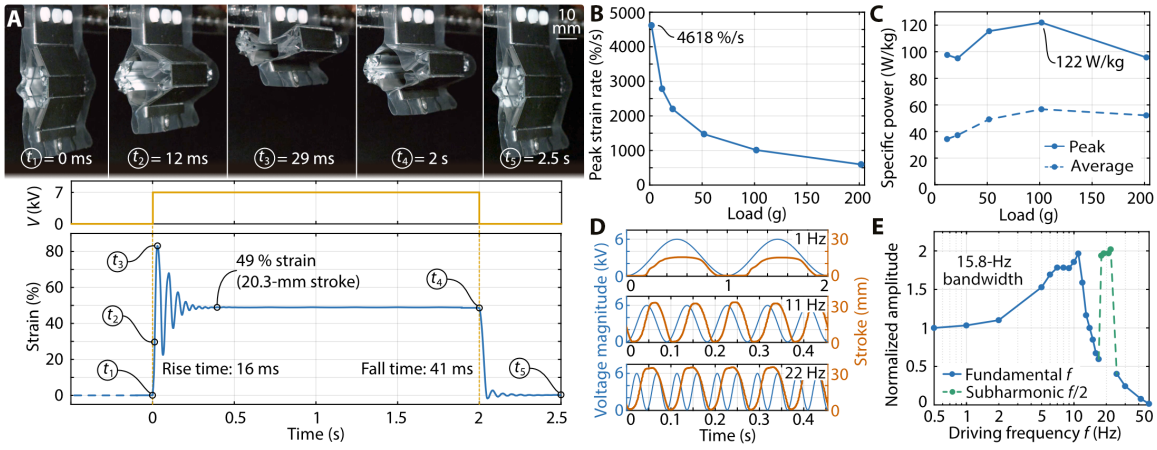

Fig. 2. Dynamic contraction of HEXEL modules. (**A**) The module exhibited fast actuation (16-ms rise time), high strain (49%), and fast relaxation (41-ms fall time) in response to a high-voltage square wave. The scale bar is 10 mm long. Further characterization of the actuation response to square-wave signals with various loads revealed (**B**) a peak strain rate of 4618%/s and (**C**) a peak specific power of 122 W/kg. (**D** and **E**) Frequency analysis revealed a bandwidth of 15.8 Hz with subharmonic actuation behavior from 17 to 25 Hz, where the actuation frequency was half of the driving frequency.

the dielectrics, causing the solid dielectrics to zip together over length z and forcing the liquid dielectric into the electrode-free region of the pouch. Because of the incompressibility of the liquid dielectric, the cross-sectional area A stayed constant throughout the actuation and is described by Eq. 1

$$A = \frac{l^2}{8\alpha^2}(2\alpha - \sin(2\alpha)) + \frac{1}{4}\sqrt{\left(c^2 + \left(L_1 - z\right)^2 + L_2^2\right)^2 - 2\left(c^4 + \left(L_1 - z\right)^4 + L_2^4\right)} \quad (1)$$

where the chord length of the film c is given by Eq. 2

$$c = \sqrt{\left(L_1 - z + L_2\cos(\theta)\right)^2 + L_2^2\sin^2(\theta)} \quad (2)$$

and $l = L_1 + L_2 + \Delta L - z$ is the arc length where ΔL is the elastic extension of the pouch defined by Eq. 3

$$\Delta L = \frac{c\alpha}{\sin(\alpha)} + z - \left(L_1 + L_2\right) \quad (3)$$

where 2α is the central angle of the electrode-free pouch region (*26*).

To find the equilibrium state of the HEXEL module, we minimized its Helmholtz free energy. When charges Q flow from the voltage source onto the electrodes of a quadrant at voltage V, the free energy of the voltage source decreases by $F_v = QV$. We idealized each actuator (one per quadrant) as a parallel plate capacitor that stores electrical energy F_c defined by Eq. 4

$$F_c = \frac{Q^2}{2C} \quad (4)$$

The capacitance C of the zipped region of each actuator is given by Eq. 5

$$C = \frac{\varepsilon_0\varepsilon_r wz}{2t_{film}} \quad (5)$$

where ε_0 is the vacuum permittivity, ε_r is the relative permittivity of the film, and t_{film} is the thickness of the film. We assumed that the zipped region had no liquid dielectric left between the films and ignored the capacitance of the unzipped region. The films at the bending sites of the quadrant (ends of plate 1) can be treated as torsional springs with free energy from bending F_b given by Eq. 6

$$F_b = \frac{1}{2}k_b\theta^2 \quad (6)$$

with bending stiffnesses k_{b1} and k_{b2}, which we calculated on the basis of the material properties of the film (see Supplementary Materials and Methods and fig. S4), leading to F_{b1} and F_{b2}. We defined the contribution to the free energy because of the elasticity of the pouch, as well as the additional effect of some degree of delamination of the pouch from the stiff plates, using Eq. 7 (*26*)

$$F_l = \frac{1}{2}k_l\Delta L^2 \quad (7)$$

k_l is difficult to precisely calculate, so we treated it as a fitting factor. We modeled the potential energy of the mass of each quadrant using Eq. 8

$$F_q = m_q g\Delta h_q \quad (8)$$

where m_q is the mass of the quadrant, g is the gravitational constant, and Δh_q is the stroke of the quadrant given by Eq. 9.

$$\Delta h_q = \left(L_1 + L_3\right)(1 - \cos(\theta)) \quad (9)$$

Similarly, the load lifted by the entire module has potential energy given by Eq. 10

$$F_m = m_l g\left(2\Delta h_q\right) \quad (10)$$

where m_l is the mass of the applied load.

On the basis of the described energetic contributions, the Helmholtz free energy of the entire module, which consists of four quadrants, is given by Eq. 11

$$F(Q, z, \alpha, \theta) = -4F_v + 4F_c + 4F_{b1} + 4F_{b2} + 4F_l + 4F_q + F_m \quad (11)$$

Downloaded from https://www.science.org at Max Planck Society on September 23, 2024

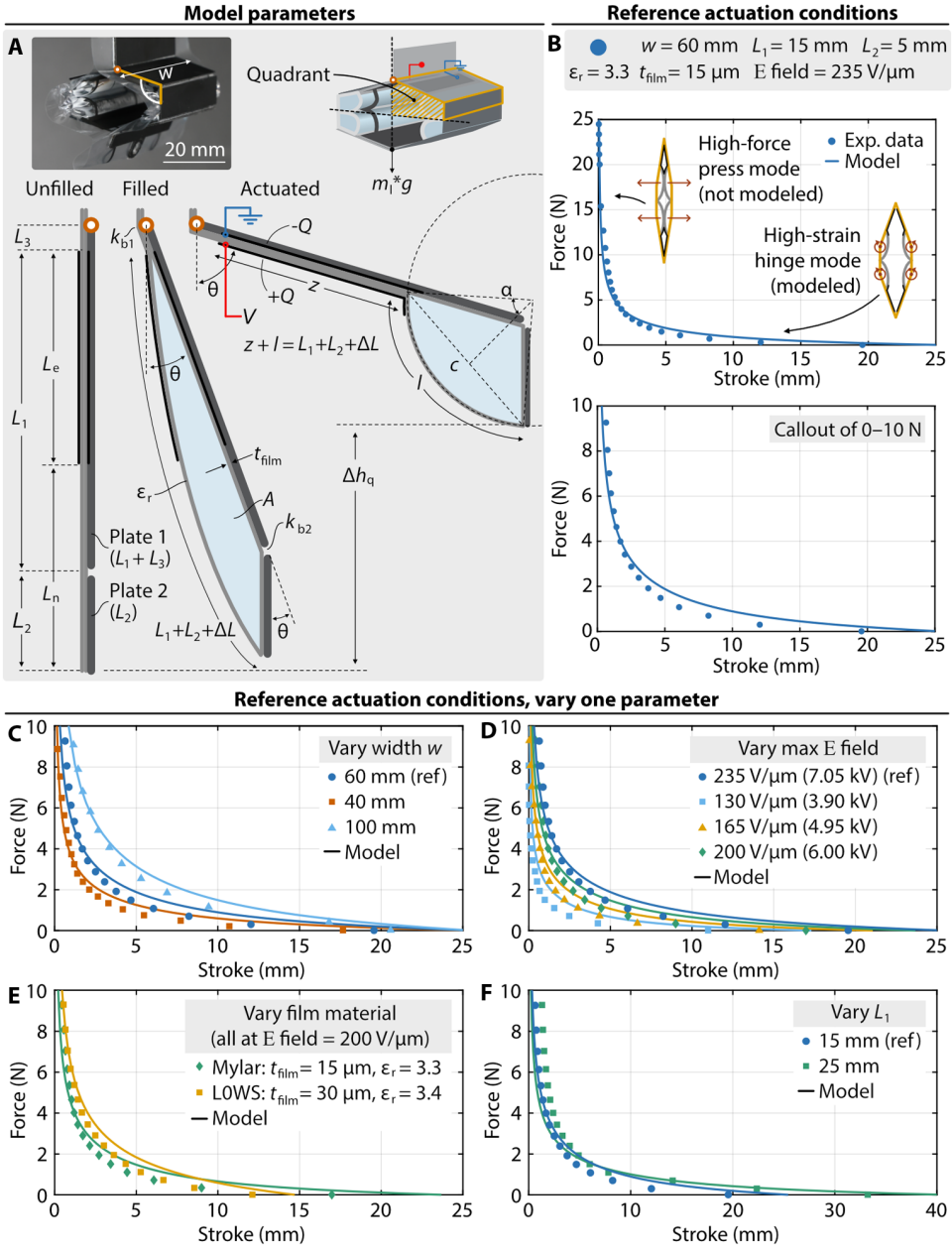

Fig. 3. Modeling the contractile force-stroke behavior of HEXEL modules. (**A**) Model parameters for one quadrant of a HEXEL module; each module consists of four quadrants. (**B**) Experimental force-stroke data for the reference actuation conditions and model predictions. For the region above 5 N of applied force, the module outperformed the model because of a secondary actuation mode in which the pouches are internally pressed against each other (unmodeled press mode) rather than hinging at the joints (modeled hinge mode). The model fits the experimental data well over various (**C**) module widths, (**D**) maximum applied electric fields, (**E**) film materials, and (**F**) plate lengths.

We numerically minimized Eq. 11 under the constraints $0 < z < L_e$ and $\theta > 0$ to calculate the equilibrium stroke of the module ($2\Delta h_q$) as a function of the applied load and voltage (all numerical values of the parameters used in the model are summarized in table S1).

Force-stroke curve and model validation

We experimentally validated this model by fabricating HEXEL modules with various parameters (summarized in table S1). We first analyzed the reference geometry, which demonstrated output forces of 0.7 N at 8.2-mm stroke (20.1% strain), 1 N at 6.1-mm stroke (14.8% strain), 3.4 N at 2.0-mm stroke (5.0% strain) (Fig. 3B), and 36.7-N blocking force (fig. S5), resulting in an average specific energy of 2.3 J/kg. We tested three HEXEL modules with this geometry and found very little deviation among the samples (maximum standard deviation in stroke of 0.3 mm for all tested forces; fig. S6).

We further tested modules of different widths w (Fig. 3C), maximum applied electric fields $\frac{V}{2t_{film}}$ (Fig. 3D), film materials (Fig. 3E), and plate lengths L_1 (Fig. 3F) and collected their force-stroke curves. Across all of the tested parameters, we found that the model captured the influence of key design parameters very well. In the low-force region (<5 N of applied force for the reference module), actuation was driven primarily by rotation at the joints (which we call hinge mode; Fig. 3B). The model consistently overpredicted the stroke for a given force in this region likely because of neglected additional elastic effects (bending of the plates) or constraints (buckling of the film because of the heat seals). In the high-force region (>5 N of applied force for the reference module), the modules exhibited a secondary actuation mode, which we call press mode (Fig. 3B and fig. S7). In press mode, as the pouches changed shape, they internally pressed against each other, creating more stroke and enabling higher blocking forces than predicted by the model. Although our model did not account for this secondary actuation mode, it agreed well with the experimental results in this regime.

The high-stroke actuation of HEXEL modules enables a wide workspace for roboticists, and our model shows that their force-stroke performance can be further tailored for various applications. Wider modules (Fig. 3C) and higher applied electric fields (Fig. 3D) enable stronger actuation, but the maximum electric field is limited by the dielectric breakdown strength of the materials system.

Thicker films have increased bending stiffness, limiting the maximum bending angle and thus the maximum stroke of the module, but they can also store more energy for the same electric field, enabling stronger actuation at low bending angles (Fig. 3E). Thicker films also require a higher magnitude of applied voltage to achieve the same electric field, and we found that the 30-μm-thick film consistently broke down at 235 V/μm (14.1 kV), thus requiring us to reduce the maximum applied electric field to 200 V/μm (12 kV).

Downloaded from https://www.science.org at Max Planck Society on September 23, 2024

We found that a plate length L_1 of 15 mm (which we used for the reference geometry) provided a well-blended performance of high free stroke and high forces. However, modules with longer plate lengths, such as the 25-mm-long version, produced even higher free stroke—up to 33.2 mm (Fig. 3F). Our model also predicted higher actuation forces with increasing film permittivity (fig. S8). Making soft electrohydraulic actuators from high-permittivity films with high dielectric breakdown strength remains an important challenge (*71*).

Characterization of lifetime

The lifetime of electrohydraulic actuators depends on a very wide range of parameters, including (but not limited to) the constitution of the driving voltage signal (polarity, amplitude, frequency, and waveform), material properties of the dielectrics (dielectric breakdown strength and defect concentration), and fabrication processes (*55*). We investigated the lifetime of HEXEL modules under typical operating conditions (room temperature, ambient humidity, 6-kV voltage amplitude, and 2-Hz sine wave) and found that a reference HEXEL module exceeded 130,000 cycles without failure (the module still had not failed when we stopped the test at 131,066 cycles), representing more than 18 hours of cyclic actuation (fig. S9, A and B). This demonstrated that the lifetime of HEXEL modules is already easily sufficient for use in academic settings and potentially for industrial use [commercial HASEL actuators can already exceed several millions of cycles (*74*)].

For the test, we used a single-polarity driving voltage signal, which resulted in decreasing stroke over time because of charge accumulation effects (fig. S9, A and B); this effect could be eliminated by careful selection of solid and liquid dielectric materials (*75*). When the module rested between days of testing, it returned to its original stroke. Reversing the polarity of the driving signal for alternating actuation cycles eliminated the stroke reduction (fig. S9C) but led to substantially shorter lifetimes (3284 and 2538 cycles under 6 kV; 7812 cycles under 5 kV; fig. S9D). The mechanism by which reversing polarity reduces the lifetime of HEXEL modules is not yet understood and should be further investigated.

Robots driven by individual HEXEL modules

The performance metrics exhibited by HEXEL modules enable agile robotic systems. We exploited the high-speed and high-strain actuation of a single HEXEL module to design a jumping robot (Fig. 4A, movie S4, and fig. S10), which jumped more than four times its relaxed height (69.7 mm at 9 kV). The electrical leads of the jumping robot initially contacted copper pads that were fixed to a table. When we applied a high-voltage pulse to the pads, the fast lateral expansion of the module led to an upward acceleration of its center of mass, propelling the robot into the air and breaking contact with the pads. Higher applied voltages led to higher jump heights (Fig. 4B), and we increased the applied voltage until dielectric breakdown occurred.

We also took advantage of the simultaneous longitudinal contraction and lateral expansion behavior of HEXEL modules to create a crawling robot capable of traversing through confined spaces (Fig. 4C, figs. S11 and S12, and movie S5). Composed of a series arrangement of three independently controlled HEXEL modules, the crawler followed a prescribed voltage pattern, which resulted in peristaltic motion (Fig. 4D). Each module expanded laterally to pull the trailing modules forward while maintaining its own position by pressing against the walls (see fig. S13 for the force-stroke curve in expansion mode). Upon relaxation, the modules returned to their original length, which enabled forward crawling.

We characterized the performance of the crawling robot about various widths of the confined space, as well as step time in the peristaltic cycle (Fig. 4, E and F). A wider gap allowed for a larger shape change in modules, resulting in faster locomotion. Lower step times also generally increased crawling speeds, leading to a peak reported speed of 19.9 mm/s. The locomotion speed decreased at the lowest step time and widest gap because the highly dynamic actuation of the modules led to poor contact with the walls. The exterior of the crawling robot presented a useful design space, and we adhered sandpaper to the surfaces that contacted the walls, which increased friction and enabled uphill crawling at angles up to 19° (Fig. 4G).

Reconfigurable HEXEL modules with magnetic connections

We designed the geometry of HEXEL modules to be symmetric and self-contained, thereby enabling each module to serve as a building block in honeycomb-like lattices that are capable of multimodal actuation (Fig. 5). We developed a rapid and reversible magnetic connection scheme between modules; these magnetic connections served a dual purpose of mechanically linking neighboring modules and providing the electrical connections necessary for control and power (Fig. 5, A and B).

We embedded magnets into the stiff plates and the ends of the high-voltage electrodes (fig. S14). The magnets in the stiff plates provided a self-aligning and reversible mechanical connection to neighboring modules (at least 3 N of connection force; Fig. 5B), as well as to additional magnetic accessories, which can enable further capabilities. These plates also created a common electrical ground by forcing contact of exterior copper leads between neighboring modules. The magnetic high-voltage lead of each module can be connected selectively to different neighbors and power supply channels, thereby providing a method of discrete control over individual modules or groups of interconnected modules. Modules can be independently controlled without interfering with neighboring units because the high voltage of each actuator is contained to the inside electrodes.

To compare the performance of the reconfigurable modules to the HEXEL modules without magnetic connections, we measured the force-strain curve of a representative reconfigurable module (Fig. 5C). Both modules showed similar performance, with the reconfigurable module reaching a lower free strain (43% as opposed to 47.7% free strain) because of the added weight of the magnets. The reconfigurable module lost connection with the magnetic mounts at an applied force of 4.1 N; larger magnets introduced the trade-off between providing a stronger connection and contributing to higher weight, as well as reducing the ease of manual disassembly.

Reconfigurable HEXEL arrays offer actuation features beyond their capabilities as individual units, and neighboring modules can connect and disconnect in seconds (on average, we connected and disconnected modules in about 3 s). For tasks requiring large displacements, for example, we created a long array of multiple HEXEL modules, which increased the overall stroke from 13.8 to 39.7 mm (Fig. 5D and movie S6). We then rearranged the same six HEXEL modules into a multimodal active array, with the left and right sides controlled independently (Fig. 5E and movie S6). We could, therefore, address either side or the entire array, and we showcased the benefits of this multimodal actuation behavior by controlling an end-effector throughout a wide spatial range.

Downloaded from https://www.science.org at Max Planck Society on September 23, 2024

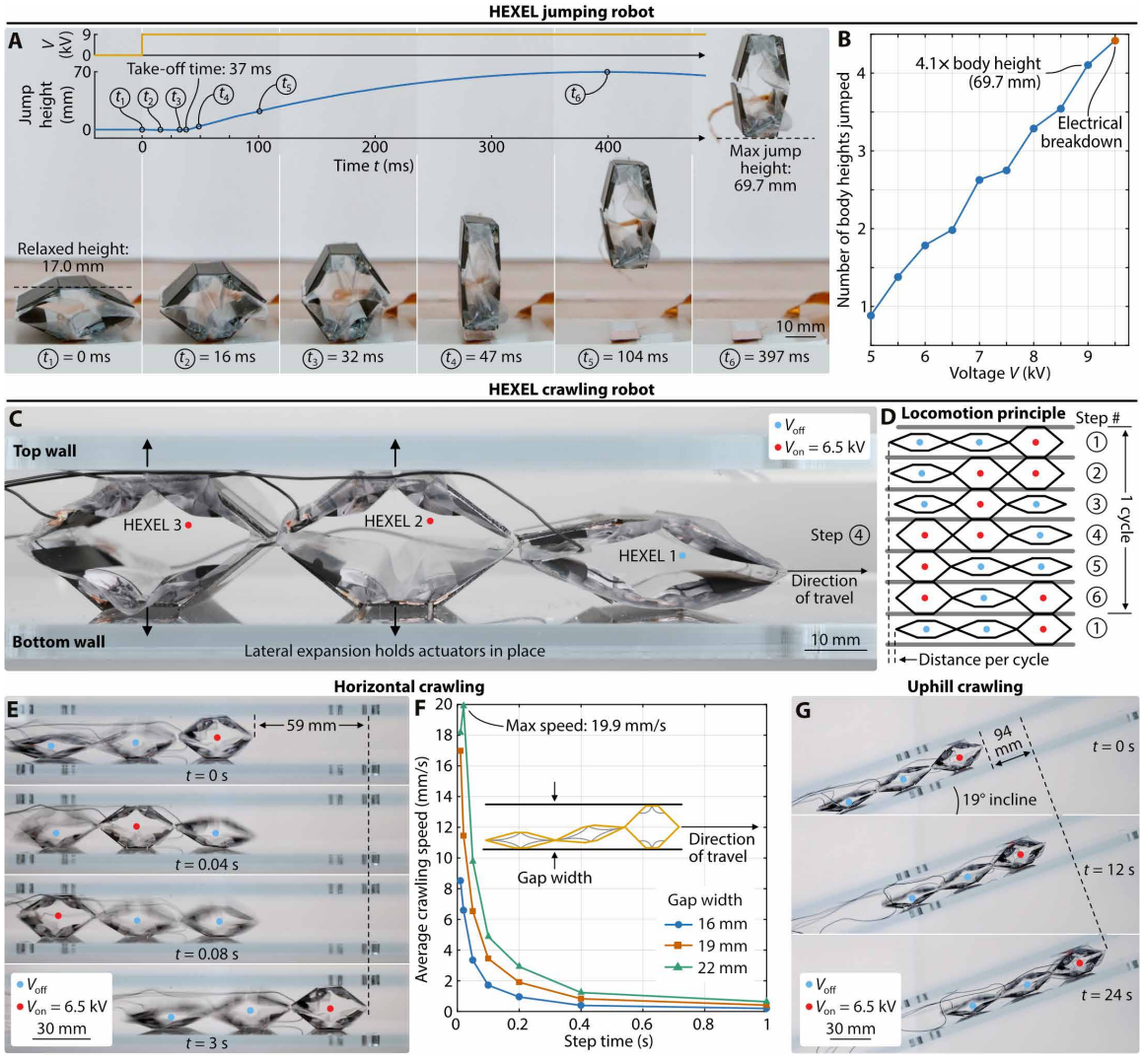

Fig. 4. Robots driven by HEXEL modules. (**A**) A jumping robot consisting of a single HEXEL module leaped more than four times its relaxed height when actuated with a 9-kV square-wave signal. (**B**) Jump height increased with applied voltage. (**C**) A robot composed of three HEXEL modules in series crawled through a confined space using (**D**) a six-step peristaltic locomotion pattern. The lateral expansion of the modules held the robot in place, whereas the linear contraction pulled trailing modules forward. The blue dots represent voltage off, and the red dots represent voltage on. (**E** and **F**) The crawling robot moved quickly through flat spaces, achieving a maximum speed of 19.9 mm/s. (**G**) We added sandpaper to the exterior of the plates to increase friction, enabling uphill crawling. The scale bars are 10 mm long in (A) and (C) and 30 mm long in (E) and (G).

In this hanging orientation, the maximum array size was limited by the number of modules connected in series because the increased weight of the modules below will eventually prevent the actuation of the top unit. Using our presented model, as well as the weight of each reconfigurable module (15.0 g), we calculated that the weight of 24 additional modules in series would constrain the top module to less than 5% strain under quasi-static conditions.

Outside of the hanging orientation, the multimodal actuation provided by each module enabled configurations with further capabilities. We arranged four modules into an active platform that used the expansion capability of HEXEL modules to raise and tilt an end-effector throughout a large spatial range (Fig. 5F and movie S7). We deconstructed this platform and magnetically connected a rounded attachment to one of the short plates for each of the four HEXEL modules (Fig. 6A, fig. S15, and movie S8). We attached these modules in a circular orientation (Fig. 6B) and demonstrated a rolling robot that exploited both the fast shape change in individual units and the independent control of modules to rapidly shift the center of mass of the robot and induce rolling (Fig. 6C), reaching peak speeds of 267 mm/s on a horizontal solid surface (Fig. 6D). The powerful actuation coupled with the inherent adaptability of each module enabled the rolling robot to traverse through sand at 250 mm/s (Fig. 6E) and to roll over rocks (Fig. 6F). We compare robotic locomotion speed as well as other parameters across a variety of soft reconfigurable modules in table S2.

Untethered, snap-on driving electronics module (snap-supply)

Thus far, we powered HEXEL modules using bench-top high-voltage amplifiers because of their robust and simple operation.

Downloaded from https://www.science.org at Max Planck Society on September 23, 2024

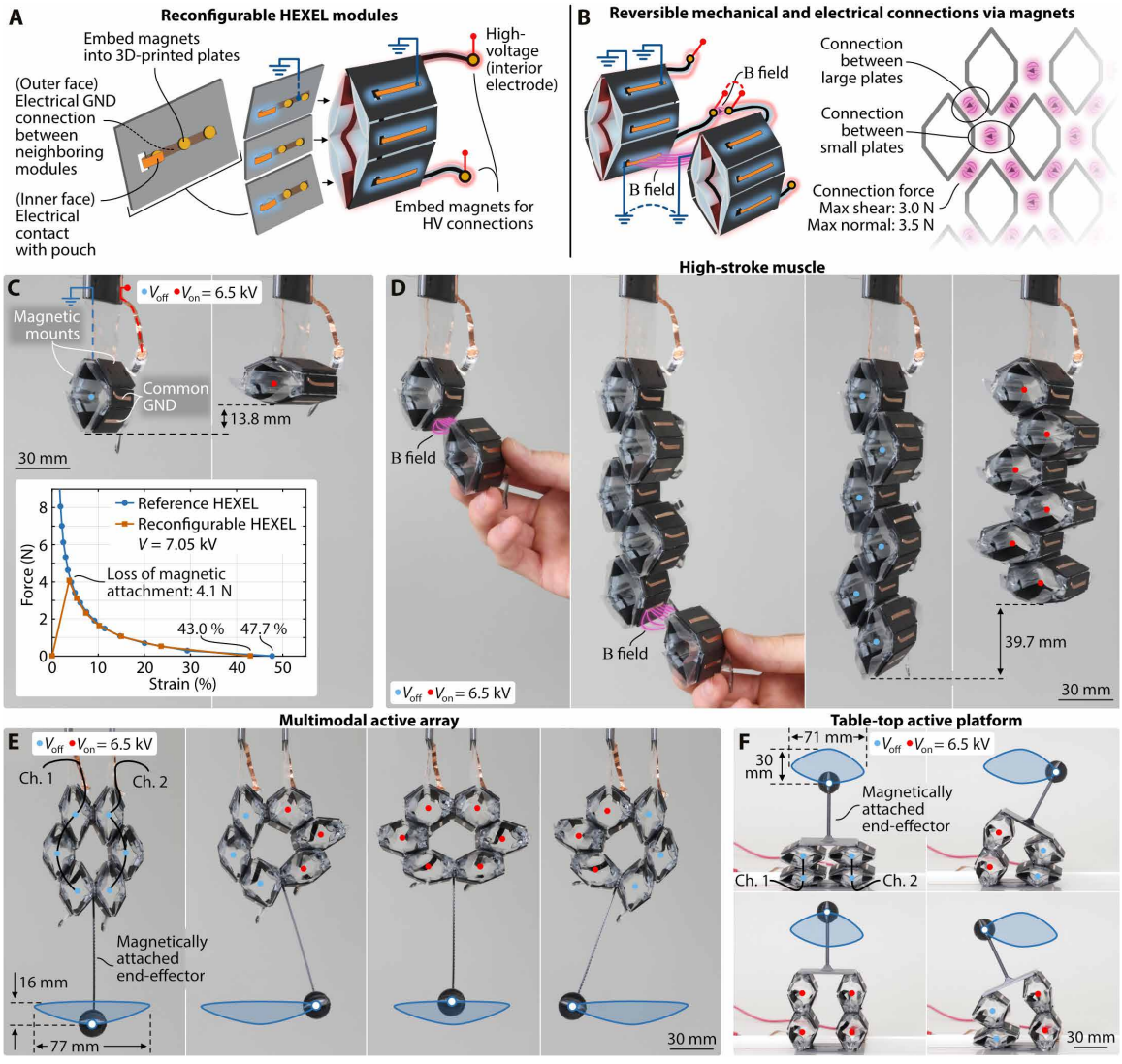

Fig. 5. Reconfigurable HEXEL modules with magnetic connections. (**A** and **B**) We embedded magnets into the stiff plates and high-voltage leads of the modules to form electrical and mechanical connections between neighboring units. (**C**) Modules exhibited force-stroke performance similar to that of their nonreconfigurable counterparts up to the limit imposed by the strength of the magnetic connections (4.1 N). (**D**) We arranged reconfigurable HEXEL modules into a high-stroke muscle. (**E**) We rearranged the modules into a multimodal active array, which controlled an end-effector throughout a wide spatial range. (**F**) We further arranged four modules into a table-top active platform, which used the lateral expansion mode. All scale bars are 30 mm long.

However, these amplifiers are heavy and bulky, therefore limiting our ability to exploit the lightweight and compact design of HEXEL modules for mobile or untethered robots. At the same time, the electrical driving mode of HEXEL modules is readily compatible with untethered, compact, battery-powered driving electronics [such as the example presented in (*52*)], and the rigid plates with embedded magnets comprising the hexagonal exoskeleton of each module provide a platform for hosting such systems.

We designed a prototypical untethered, snap-on driving electronics module, called a snap-supply, that magnetically attaches to one of the plates of HEXEL modules and drives their actuation (Fig. 7 and movie S9). Each snap-supply shares a footprint (50.0 mm by 18.2 mm by 9.1 mm; Fig. 7, A and B) similar to that of the large plates of HEXEL modules and uses off-the-shelf components, including a high-voltage dc-dc converter, a 95-mA·hour battery, a high-voltage optodiode for discharging, and a printed circuit board (Fig. 7, B and C, fig. S16, and table S3). The printed circuit board contains an electrical circuit that provides a square-wave driving signal at a fixed frequency of 0.53 Hz at a maximum voltage of 6.7 kV (enabling up to 44 min of run-time when driving a reference-geometry HEXEL module).

We first characterized the slew rate of the snap-supply when driving HEXEL modules (Fig. 7D and fig. S17A) and found charging speeds that ranged from 182 ms for one module to 494 ms for four modules. This resulted in a peak contraction-mode strain rate of 1004%/s and a peak expansion-mode strain rate of 2614%/s for one module (fig. S17B). The discharging is controlled by the optodiode, enabling higher slew rates (fig. S17A) and therefore faster discharging

Downloaded from https://www.science.org at Max Planck Society on September 23, 2024

Fig. 6. Rolling robot composed of reconfigurable HEXEL modules. (**A** and **B**) Magnetic accessories can be easily added to increase the application space of reconfigurable HEXEL modules. Here, we added rounded magnetic attachments to create a rolling robot. (**C**) The robot rolled by rapidly shifting its center of mass. (**D**) The robot reached average translation speeds of 267 mm/s on a solid surface and (**E**) 250 mm/s in sand. (**F**) The fast actuation and conformal nature of each HEXEL module enabled the robot to jump and roll over rocks. The scale bars are 40 mm long in (B) and 30 mm long in (D) to (F).

times than during charging (as little as 54 ms for one module; Fig. 7D). The snap-supply can drive many modules at once (Fig. 7, E and F) and weighs only 12.5 g (similar in weight to one reconfigurable HEXEL module); HEXEL modules can therefore easily lift their own driving electronics in both linearly contracting and laterally expanding actuation modes (fig. S18).

DISCUSSION

Here, we introduced a versatile and scalable framework for designing reconfigurable robots composed of modules driven by soft electrohydraulic actuators. By coupling these soft actuators with rigid components, HEXEL modules achieved high strain and fast actuation, and their hexagonal form factor and integrated magnetic connection scheme allowed repeating arrays of modules to be rapidly assembled into reconfigurable robotic systems. Executing multiple tasks with the same group of modules promotes versatility, reduces both cost and environmental footprint, and provides potential solutions for resource- or payload-limited environments (*76*).

The use of rigid plates offers each HEXEL module capabilities beyond fully soft actuators. In addition to amplifying the stroke, plates can serve as exoskeletons for protecting soft actuator components from their surroundings or the surroundings from the high-voltage electrodes, and the soft joints and actuators provide semiconformability and back-drivability. In addition, plates offer workspaces not only for embedding connection mechanisms but also for hosting additional sensing, communication, and computation components; here, we leveraged these workspaces for hosting an untethered,

Downloaded from https://www.science.org at Max Planck Society on September 23, 2024

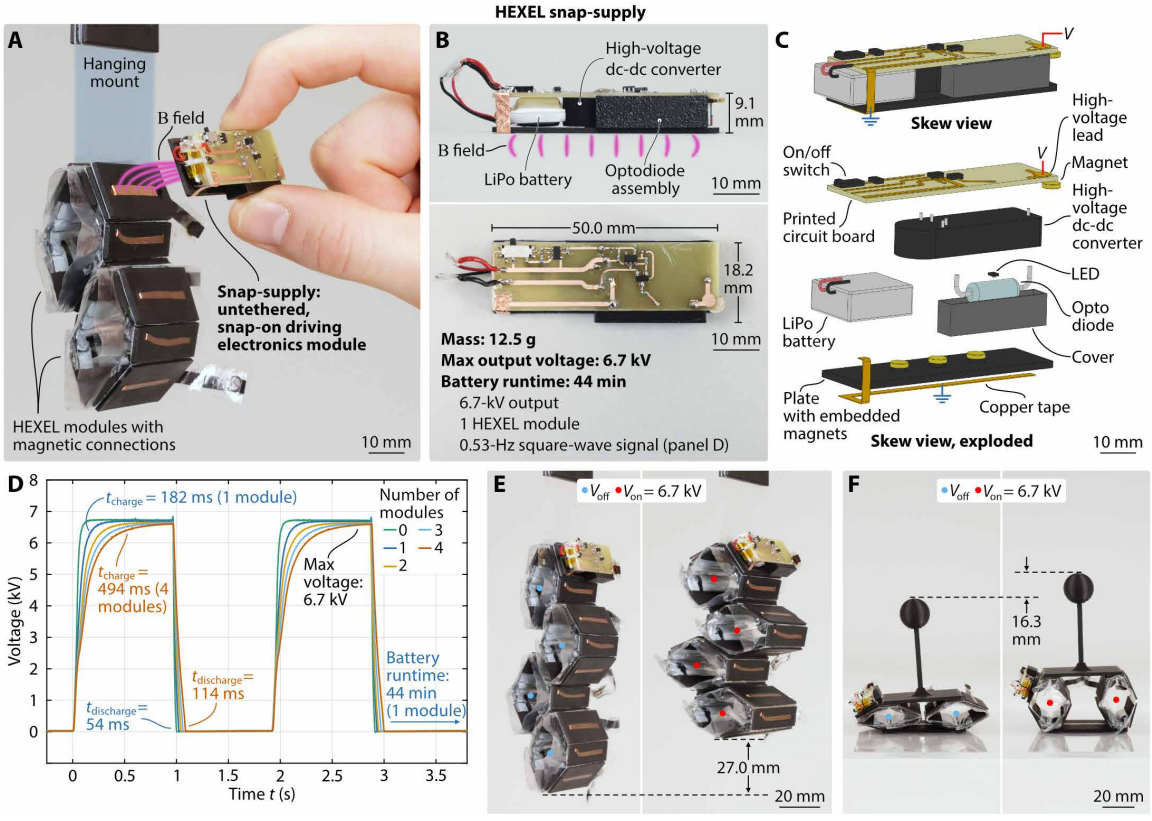

Fig. 7. Untethered, snap-on driving electronics module (snap-supply). (**A**) The magnetic plates of HEXEL modules offer a workspace for hosting additional components, such as compact, battery-powered driving electronics. (**B** and **C**) The snap-supply has a compact and lightweight form factor and uses off-the-shelf components. (**D**) One snap-supply is capable of driving multiple HEXEL modules, with the slew rate depending on the number of modules driven. (**E** and **F**) The snap-supply can drive HEXEL modules in both contraction and expansion actuation modes. The scale bars are 10 mm long in (A) to (C) and 20 mm long in (E) and (F).

onboard driving electronics module that magnetically snaps onto HEXEL modules and drives their actuation. This driving electronics module features a simple design using off-the-shelf components, yet enables high operating voltages, fast actuation speeds, and a battery run-time sufficient for many robotics tasks. Our prototypical design is currently limited by the hardware-defined actuation pattern, and more versatile actuation behavior could be enabled by integrated microcontrollers with wireless communication. In addition, our design cannot provide the bursts of power required for jumping actuation—alternative high-voltage dc-dc converters with higher power output (*77*) or the use of buffer capacitors that can rapidly release stored charge could enable such dynamic behavior. Together, our modular architecture could enable highly distributed systems that leverage the large shape change, fast actuation speeds, and modular design of HEXEL modules; examples include active surfaces that rapidly adjust to surrounding environmental parameters such as light reflection and aerodynamics, as well as electrohydraulic energy harvesters (*57*, *78*) that meet calls for small-scale, distributed renewable energy generation (*79*, *80*).

As individual actuators, HEXEL modules offer unique performance benefits when compared with state-of-the-art soft electrohydraulic actuators. Compared with linearly contracting Peano-HASEL actuators, HEXEL modules exhibit lower blocking forces but much higher contractile strains (*54*, *63*), offering substantial advantages for biomimetic robotic systems in which small actuation strokes would be largely dissipated by lossy transmission systems (we compare the performance of HEXEL modules with that of other thermoplastic-based HASEL actuators in table S4). Linearly contracting electroribbon artificial muscles (*58*, *62*) provide very high contractile strain and higher specific energy than HEXEL modules, but HEXEL modules in place offer substantially higher actuation speeds and increased practicality for robotic integration because of their closed fluidic packaging as well as their standalone modular design. In comparison with electrostatic bellow muscle actuators (*57*), which also feature stackable, high-strain actuation, HEXEL modules exhibit higher free strain, faster peak actuation speed, and a modular design without the need for a stretchable external oil reservoir.

Although individual HEXEL modules already exhibit attractive actuation capabilities, their specific energy (2.3 J/kg) could be further increased to enable stronger robots. As elucidated in the presented model, the specific energy could be increased by using films with higher relative permittivity and higher dielectric breakdown strength; film thickness and plate length could be additionally optimized to provide higher strains or higher forces according to the desired application.

Exploring the physical downscaling of HEXEL modules could enable densely packed, higher-resolution arrays with increased complexity of motion and better integration into small robots and wearable devices. The HEXEL modules presented here can be stacked in plane; the key design principles could be further expanded for modules that additionally enable out-of-plane stacking, adding

Downloaded from https://www.science.org at Max Planck Society on September 23, 2024

another degree of freedom to the reconfigurable arrays, thereby enabling an even wider application space.

However, large arrays of HEXEL modules carry their own limitations. Closely packed modules could constrain neighboring units and reduce their range of motion, although additional passive fixtures between neighbors could help to reduce these constraints. In addition, when arrays are in a vertical orientation, each additional module in the series increases the applied load to the modules above, thus reducing their actuation strain. Arrays comprising a large number of HEXEL units provide opportunities for more complex behavior, and the untethered, snap-on driving electronics module presented here provides a method of controlling each group of modules independently and without the need for bulky external high-voltage amplifiers.

Autonomous self-assembly is an exciting prospect for reconfigurable robots, and HEXEL modules with onboard, untethered driving electronics could, in principle, serve as modular units that interact with neighbors to grow and change shapes, enabling collective behaviors. Our choice to connect units with magnets, however, currently prevents the self-assembly of HEXEL robots because it necessitates manual assembly and disassembly. There are a variety of controllable attachment methods that could be implemented into HEXEL modules, including mechanical hooks and pins (*17*), though at the cost of increased weight and system complexity. Overall, HEXEL modules leverage the benefits of both soft electrohydraulic actuators and rigid reconfigurable modules for designing versatile, robust, and cost-effective robots.

MATERIALS AND METHODS

Module materials

We used two thermoplastic films for fabricating the soft electrohydraulic actuators: 15-μm-thick polyester film (Mylar Petroplast 850H, DuPont) and 30-μm-thick polyester film (L0WS HSF4000W, Multiplastics Europe), both with a one-sided heat-sealing layer. For all actuators, we used 5-centistoke (cSt)–viscosity silicone oil as the liquid dielectric (Silicone Oil M5, Carl Roth). We used 0.5-mm-thick fiberglass plates for the standalone HEXEL modules (0.5-mm-thick FR4, RS Pro) and 3D-printed nylon plates (Onyx filament, MarkForged Onyx One) for the HEXEL modules with embedded magnets (neodymium magnets, SM-04x01-G, magnets4you). For the external ground connections of the HEXEL modules, we used copper tape (Oubaka). The fabrication processes for all HEXEL modules and demonstrations are described in detail in Supplementary Materials and Methods.

For our reference HEXEL module geometry, we used 60-mm-wide by 20-mm-tall pouches to remain consistent with existing literature (*47*, *54*, *56*, *71*, *73*). We made each pouch from 15-μm-thick polyester film and filled each with 1.9 ml of 5-cSt silicone oil.

Testing methods

Dynamic characterization

To characterize the dynamics of HEXEL modules without magnetic connections, we applied various driving signals using a custom MATLAB (R2021a) program, which communicated with a high-voltage amplifier (TREK 50/12, Advanced Energy) and an indicator light-emitting diode (LED) via a data acquisition (DAQ) device (USB-6212, National Instruments). We recorded the response with a high-speed camera (Phantom v2640, Vision Research) at a frame rate of 2000 or 5000 fps. We used the LED to sync the recorded video with the application of high voltage and used tracking software (Tracker version 6.1.2, Open Source Physics) to measure the stroke of the modules. For Fig. 2 (B, C, and E), we connected consecutive, discrete data points with a visual linear guideline.

Force-stroke curves

To collect the force-stroke curves of HEXEL modules without magnetic connections, we used a custom MATLAB program, which communicated with a high-voltage amplifier (TREK 610E, Advanced Energy) and a dual-mode muscle lever (310C-LR, Aurora Scientific) via a DAQ (USB-6212, National Instruments). We used the high-voltage amplifier to drive actuation and the dual-mode muscle lever to record the resulting force and stroke of the HEXEL modules.

We attached the modules to the arm of the dual-mode muscle lever, which stepped through a range of prescribed forces. At each force step, high-voltage, ramped square waves (50-ms ramp time) were applied, and the position of the arm was recorded. For each actuation cycle, we calculated the difference between the maximum and minimum position of the arm to determine the stroke of the module for that cycle. For each force step, we then took the average stroke of the first two actuation cycles. To characterize the stroke of the module under no load, we recorded the response with a camera (Canon EOS R5) and tracked the displacement using the same tracking software.

We first measured force-stroke curves for three reference modules, which exhibited low deviation among samples (maximum SD in stroke of 0.3 mm for all tested forces; fig. S6), thus confirming repeatable fabrication and performance. Therefore, for all other force-stroke curves, we tested one representative module.

For all modules except the 30-μm-thick L0WS module, we used a reversing polarity voltage signal. The 30-μm-thick L0WS module consistently broke down under reversing polarity voltage signals but repeatedly actuated without failure under single polarity conditions.

Characterization of demonstrations

For the jumping robot, crawling robot, reconfigurable arrays in Fig. 5, and rolling robot, we applied the driving signals with high-voltage amplifiers (TREK 610E, Advanced Energy) and measured displacements and speeds by recording motion with a camera (Canon EOS R5). For the reconfigurable arrays in Fig. 7, we applied the driving signals with the snap-supply and measured displacements and speeds by recording motion with a high-speed camera (Phantom v2640, Vision Research) at a frame rate of 1000 fps. For both driving methods, we tracked the position of interest using the same tracking software (Tracker version 6.1.2, Open Source Physics). For Fig. 4 (B and F) and Fig. 5C, we connected consecutive, discrete data points with a visual linear guideline.

Statistical analysis

For the analysis of the actuation frequency of HEXEL modules (Fig. 2E), we calculated the mean displacement of consecutive actuation cycles. For actuation frequencies that did not produce out-of-plane instabilities, we computed the mean displacement of five cycles. For the actuation frequencies that did produce out-of-plane instabilities (6 to 9 Hz and 18 to 19 Hz), the instability dominated after a few cycles, so we used only the first cycles where actuation was stable to calculate the amplitude; we computed the mean displacement using the first three cycles for 6, 8, 9, 18, and 19 Hz and the first two cycles for 7 Hz.

For all force-stroke curves, we computed the mean displacement of the first two consecutive actuation cycles for each prescribed

Downloaded from https://www.science.org at Max Planck Society on September 23, 2024

force. For the force-stroke curve in fig. S6, we computed the means and SD of the displacement of three reference HEXEL modules for each prescribed force. All other experiments used one representative sample.

Supplementary Materials

The PDF file includes:
Materials and Methods
Figs. S1 to S18
Tables S1 to S4
References (*81*–*83*)

Other Supplementary Material for this manuscript includes the following:
Movies S1 to S9

REFERENCES AND NOTES

1. J. Kober, J. A. Bagnell, J. Peters, Reinforcement learning in robotics: A survey. *Int. J. Robot. Res.* **32**, 1238–1274 (2013).
2. D. Rus, M. T. Tolley, Design, fabrication and control of soft robots. *Nature* **521**, 467–475 (2015).
3. A. Brunete, A. Ranganath, S. Segovia, J. P. de Frutos, M. Hernando, E. Gambao, Current trends in reconfigurable modular robots design. *Int. J. Adv. Rob. Syst.* **14**, 1–21 (2017).
4. K. Gilpin, D. Rus, Modular robot systems. *IEEE Robot. Autom. Mag.* **17**, 38–55 (2010).
5. M. Yim, Y. Zhang, D. Duff, Modular robots. *IEEE Spectr.* **39**, 30–34 (2002).
6. J. Seo, J. Paik, M. Yim, Modular reconfigurable robotics. *Annu. Rev. Control Robot. Auton. Syst.* **2**, 63–88 (2019).
7. M. Yim, W.-m. Shen, B. Salemi, D. Rus, M. Moll, H. Lipson, E. Klavins, G. Chirikjian, Modular self-reconfigurable robot systems [grand challenges of robotics]. *IEEE Robot. Autom. Mag.* **14**, 43–52 (2007).
8. C. Zhang, P. Zhu, Y. Lin, Z. Jiao, J. Zou, Modular soft robotics: Modular units, connection mechanisms, and applications. *Adv. Intell. Syst.* **2**, 1900166 (2020).
9. T. Fukuda, Y. Kawauchi, Cellular robotic system (CEBOT) as one of the realization of self-organizing intelligent universal manipulator, in *Proceedings, IEEE International Conference on Robotics and Automation* (IEEE, 1990), pp. 662–667.
10. R. J. Alattas, S. Patel, T. M. Sobh, Evolutionary modular robotics: Survey and analysis. *J. Intell. Robot. Syst.* **95**, 815–828 (2018).
11. J. Baca, S. G. M. Hossain, P. Dasgupta, C. A. Nelson, A. Dutta, ModRED: Hardware design and reconfiguration planning for a high dexterity modular self-reconfigurable robot for extra-terrestrial exploration. *Robot. Auton. Syst.* **62**, 1002–1015 (2014).
12. J. Baca, M. Ferre, R. Aracil, A heterogeneous modular robotic design for fast response to a diversity of tasks. *Robot. Auton. Syst.* **60**, 522–531 (2012).
13. C. H. Belke, J. Paik, Mori: A modular origami robot. *IEEE/ASME Trans. Mechatron.* **22**, 2153–2164 (2017).
14. S. Murata, E. Yoshida, A. Kamimura, H. Kurokawa, K. Tomita, S. Kokaji, M-TRAN: Self-reconfigurable modular robotic system. *IEEE/ASME Trans. Mechatron.* **7**, 431–441 (2002).
15. H. Wei, Y. Chen, J. Tan, T. Wang, Sambot: A self-assembly modular robot system. *IEEE/ASME Trans. Mechatron.* **16**, 745–757 (2011).
16. M. Yim, D. G. Duff, K. D. Roufas, PolyBot: A modular reconfigurable robot, in *2000 IEEE International Conference on Robotics and Automation. Symposia Proceedings* (IEEE, 2000), pp. 514–520.
17. W. Saab, P. Racioppo, P. Ben-Tzvi, A review of coupling mechanism designs for modular reconfigurable robots. *Robotica* **37**, 378–403 (2019).
18. S. Kim, C. Laschi, B. Trimmer, Soft robotics: A bioinspired evolution in robotics. *Trends Biotechnol.* **31**, 287–294 (2013).
19. C. Laschi, B. Mazzolai, M. Cianchetti, Soft robotics: Technologies and systems pushing the boundaries of robot abilities. *Sci. Robot.* **1**, eaah3690 (2016).
20. G. M. Whitesides, Soft robotics. *Angew. Chem. Int. Ed.* **57**, 4258–4273 (2018).
21. P. Polygerinos, N. Correll, S. A. Morin, B. Mosadegh, C. D. Onal, K. Petersen, M. Cianchetti, M. T. Tolley, R. F. Shepherd, Soft robotics: Review of fluid-driven intrinsically soft devices; manufacturing, sensing, control, and applications in human-robot interaction. *Adv. Eng. Mater.* **19**, 1700016 (2017).
22. S. M. Mirvakili, I. W. Hunter, Artificial muscles: Mechanisms, applications, and challenges. *Adv. Mater.* **30**, 1704407 (2018).
23. J. Fang, Y. Zhuang, K. Liu, Z. Chen, Z. Liu, T. Kong, J. Xu, C. Qi, A shift from efficiency to adaptability: Recent progress in biomimetic interactive soft robotics in wet environments. *Adv. Sci.* **9**, e2104347 (2022).
24. F. Ilievski, A. D. Mazzeo, R. F. Shepherd, X. Chen, G. M. Whitesides, Soft robotics for chemists. *Angew. Chem. Int. Ed.* **50**, 1890–1895 (2011).
25. J. Shintake, V. Cacucciolo, D. Floreano, H. Shea, Soft robotic grippers. *Adv. Mater.* **30**, 1707035 (2018).
26. N. Kellaris, P. Rothemund, Y. Zeng, S. K. Mitchell, G. M. Smith, K. Jayaram, C. Keplinger, Spider-inspired electrohydraulic actuators for fast, soft-actuated joints. *Adv. Sci.* **8**, 2100916 (2021).
27. P. Rothemund, Y. Kim, R. H. Heisser, X. Zhao, R. F. Shepherd, C. Keplinger, Shaping the future of robotics through materials innovation. *Nat. Mater.* **20**, 1582–1587 (2021).
28. N. W. Bartlett, M. T. Tolley, J. T. B. Overvelde, J. C. Weaver, B. Mosadegh, K. Bertoldi, G. M. Whitesides, R. J. Wood, A 3D-printed, functionally graded soft robot powered by combustion. *Science* **349**, 161–165 (2015).
29. M. T. Tolley, R. F. Shepherd, B. Mosadegh, K. C. Galloway, M. Wehner, M. Karpelson, R. J. Wood, G. M. Whitesides, A resilient, untethered soft robot. *Soft Robot.* **1**, 213–223 (2014).
30. R. V. Martinez, A. C. Glavan, C. Keplinger, A. I. Oyetibo, G. M. Whitesides, Soft actuators and robots that are resistant to mechanical damage. *Adv. Funct. Mater.* **24**, 3003–3010 (2014).
31. Y.-L. Park, B.-r. Chen, C. Majidi, R. J. Wood, R. Nagpal, E. Goldfield, Active modular elastomer sleeve for soft wearable assistance robots, in *2012 IEEE/RSJ International Conference on Intelligent Robots and Systems* (IEEE, 2012), pp. 1595–1602.
32. S. Li, S. A. Awale, K. E. Bacher, T. J. Buchner, C. Della Santina, R. J. Wood, D. Rus, Scaling up soft robotics: A meter-scale, modular, and reconfigurable soft robotic system. *Soft Robot.* **9**, 324–336 (2022).
33. J. Zou, Y. Lin, C. Ji, H. Yang, A reconfigurable omnidirectional soft robot based on caterpillar locomotion. *Soft Robot.* **5**, 164–174 (2018).
34. R. Natividad, M. Del Rosario Jr., P. C. Y. Chen, C.-H. Yeow, A reconfigurable pneumatic bending actuator with replaceable inflation modules. *Soft Robot.* **5**, 304–317 (2018).
35. A. Vergara, Y.-S. Lau, R.-F. Mendoza-Garcia, J. C. Zagal, Soft modular robotic cubes: Toward replicating morphogenetic movements of the embryo. *PLOS One* **12**, e0169179 (2017).
36. C. Zhang, Z. Zhang, Y. Peng, Y. Zhang, S. An, Y. Wang, Z. Zhai, Y. Xu, H. Jiang, Plug & play origami modules with all-purpose deformation modes. *Nat. Commun.* **14**, 4329 (2023).
37. C. D. Onal, D. Rus, A modular approach to soft robots, in *2012 4th IEEE RAS & EMBS International Conference on Biomedical Robotics and Biomechatronics (BioRob)* (IEEE, 2012), pp. 1034–1045.
38. W. Wang, N.-G. Kim, H. Rodrigue, S.-H. Ahn, Modular assembly of soft deployable structures and robots. *Mater. Horiz.* **4**, 367–376 (2017).
39. Y. Zhou, H. Jin, C. Liu, E. Dong, M. Xu, J. Yang, A novel biomimetic jellyfish robot based on a soft and smart modular structure (SMS), in *2016 IEEE International Conference on Robotics and Biomimetics (ROBIO)* (IEEE, 2016), pp. 708–713.
40. J. K. Paik, A. Byoungkwon, D. Rus, R. J. Wood, Robotic origamis: Self-morphing modular robot, paper presented at International Conference on Morphological Computation, Venice, Italy, 12–14 September 2011.
41. D. Wang, B. Zhao, X. Li, L. Dong, M. Zhang, J. Zou, G. Gu, Dexterous electrical-driven soft robots with reconfigurable chiral-lattice foot design. *Nat. Commun.* **14**, 5067 (2023).
42. M. G. B. Atia, A. Mohammad, A. Gameros, D. Axinte, I. Wright, Reconfigurable soft robots by building blocks. *Adv. Sci.* **9**, 2203217 (2022).
43. C. Cao, R. S. Diteesawat, J. Rossiter, A. T. Conn, A reconfigurable crawling robot driven by electroactive artificial muscle, in *2019 2nd IEEE International Conference on Soft Robotics (RoboSoft)* (IEEE, 2019), pp. 840–845.
44. Q. Pei, M. Rosenthal, S. Stanford, H. Prahlad, R. Pelrine, Multiple-degrees-of-freedom electroelastomer roll actuators. *Smart Mater. Struct.* **13**, N86 (2004).
45. P. J. White, S. Latscha, S. Schlaefer, M. Yim, Dielectric elastomer bender actuator applied to modular robotics, in *2011 IEEE/RSJ International Conference on Intelligent Robots and Systems* (IEEE, 2011), pp. 408–413.
46. J. Xue, Y. Du, W. Zhao, X. Gao, A modular crawling robot driven by a single-layer conical dielectric elastomer, in *2022 IEEE International Conference on Robotics and Biomimetics (ROBIO)* (IEEE, 2022), pp. 783–788.
47. P. Rothemund, S. Kirkman, C. Keplinger, Dynamics of electrohydraulic soft actuators. *Proc. Natl. Acad. Sci. U.S.A.* **117**, 16207–16213 (2020).
48. B. K. Johnson, M. Naris, V. Sundaram, A. Volchko, K. Ly, S. K. Mitchell, E. Acome, N. Kellaris, C. Keplinger, N. Correll, J. S. Humbert, M. E. Rentschler, A multifunctional soft robotic shape display with high-speed actuation, sensing, and control. *Nat. Commun.* **14**, 4516 (2023).
49. Z. Yoder, D. Macari, G. Kleinwaks, I. Schmidt, E. Acome, C. Keplinger, A soft, fast and versatile electrohydraulic gripper with capacitive object size detection. *Adv. Funct. Mater.* **33**, 2209080 (2023).
50. T. Wang, H.-J. Joo, S. Song, W. Hu, C. Keplinger, M. Sitti, A versatile jellyfish-like robotic platform for effective underwater propulsion and manipulation. *Sci. Adv.* **9**, eadg0292 (2023).
51. S. Schlatter, P. Illenberger, S. Rosset, Peta-pico-Voltron: An open-source high voltage power supply. *HardwareX* **4**, e00039 (2018).
52. S. K. Mitchell, T. Martin, C. Keplinger, A pocket-sized ten-channel high voltage power supply for soft electrostatic actuators. *Adv. Mater. Technol.* **7**, 2101469 (2022).

Downloaded from https://www.science.org at Max Planck Society on September 23, 2024

53. E. Acome, S. K. Mitchell, T. G. Morrissey, M. B. Emmett, C. Benjamin, M. King, M. Radakovitz, C. Keplinger, Hydraulically amplified self-healing electrostatic actuators with muscle-like performance. *Science* **359**, 61–65 (2018).
54. N. Kellaris, V. G. Venkata, G. M. Smith, S. K. Mitchell, C. Keplinger, Peano-HASEL actuators: Muscle-mimetic, electrohydraulic transducers that linearly contract on activation. *Sci. Robot.* **3**, eaar3276 (2018).
55. P. Rothemund, N. Kellaris, S. K. Mitchell, E. Acome, C. Keplinger, HASEL artificial muscles for a new generation of lifelike robots—Recent progress and future opportunities. *Adv. Mater.* **33**, e2003375 (2021).
56. E. H. Rumley, D. Preninger, A. Shagan Shomron, P. Rothemund, F. Hartmann, M. Baumgartner, N. Kellaris, A. Stojanovic, Z. Yoder, B. Karrer, C. Keplinger, M. Kaltenbrunner, Biodegradable electrohydraulic actuators for sustainable soft robots. *Sci. Adv.* **9**, eadf5551 (2023).
57. I. D. Sîrbu, G. Moretti, G. Bortolotti, M. Bolignari, S. Diré, L. Fambri, R. Vertechy, M. Fontana, Electrostatic bellow muscle actuators and energy harvesters that stack up. *Sci. Robot.* **6**, eaaz5796 (2021).
58. M. Taghavi, T. Helps, J. Rossiter, Electro-ribbon actuators and electro-origami robots. *Sci. Robot.* **3**, eaau9795 (2018).
59. M. R. O'Neill, E. Acome, S. Bakarich, S. K. Mitchell, J. Timko, C. Keplinger, R. F. Shepherd, Rapid 3D printing of electrohydraulic (HASEL) tentacle actuators. *Adv. Funct. Mater.* **30**, 2005244 (2020).
60. E. Leroy, R. Hinchet, H. Shea, Multimode hydraulically amplified electrostatic actuators for wearable haptics. *Adv. Mater.* **32**, e2002564 (2020).
61. Z. Yoder, N. Kellaris, C. Chase-Markopoulou, D. Ricken, S. K. Mitchell, M. B. Emmett, R. F. F. Weir, J. Segil, C. Keplinger, Design of a high-speed prosthetic finger driven by Peano-HASEL actuators. *Front. Robot. AI* **7**, 586216 (2020).
62. S. Hoh, T. Helps, R. S. Diteesawat, M. Taghavi, J. Rossiter, Electro-lattice actuator: A compliant high-contractile active lattice structure. *Smart Mater. Struct.* **30**, 125034 (2021).
63. X. Wang, S. K. Mitchell, E. H. Rumley, P. Rothemund, C. Keplinger, High-strain Peano-HASEL actuators. *Adv. Funct. Mater.* **30**, 1908821 (2020).
64. S. K. Mitchell, X. Wang, E. Acome, T. Martin, K. Ly, N. Kellaris, V. G. Venkata, C. Keplinger, An easy-to-implement toolkit to create versatile and high-performance HASEL actuators for untethered soft robots. *Adv. Sci.* **6**, 1900178 (2019).
65. J. Ueda, T. W. Secord, H. H. Asada, Large effective-strain piezoelectric actuators using nested cellular architecture with exponential strain amplification mechanisms. *IEEE/ASME Trans. Mechatron.* **15**, 770–782 (2010).
66. G. Stone, R. Van Heeswijk, Parameter estimation for the Weibull distribution. *IEEE Trans. Electr. Insul.* **EI-12**, 253–261 (1977).
67. C. S. Haines, M. D. Lima, N. Li, G. M. Spinks, J. Foroughi, J. D. W. Madden, S. H. Kim, S. Fang, M. Jung de Andrade, F. Göktepe, Ö. Göktepe, S. M. Mirvakili, S. Naficy, X. Lepró, J. Oh, M. E. Kozlov, S. J. Kim, X. Xu, B. J. Swedlove, G. G. Wallace, R. H. Baughman, Artificial muscles from fishing line and sewing thread. *Science* **343**, 868–872 (2014).
68. S. Medler, Comparative trends in shortening velocity and force production in skeletal muscles. *Am. J. Physiol. Regul. Intgr. Comp. Physiol.* **283**, R368–R378 (2002).
69. C.-J. Cao, T. L. Hill, A. T. Conn, B. Li, X. Gao, Nonlinear dynamics of a magnetically coupled dielectric elastomer actuator. *Phys. Rev. Appl.* **12**, 044033 (2019).
70. H. Vatanjou, Y. Hojjat, M. Karafi, Nonlinear dynamic analysis of dielectric elastomer minimum energy structures. *Appl. Phys. A* **125**, 583 (2019).
71. N. Kellaris, V. G. Venkata, P. Rothemund, C. Keplinger, An analytical model for the design of Peano-HASEL actuators with drastically improved performance. *Extreme Mech. Lett.* **29**, 100449 (2019).
72. S. Kirkman, P. Rothemund, E. Acome, C. Keplinger, Electromechanics of planar HASEL actuators. *Extreme Mech. Lett.* **48**, 101408 (2021).
73. P. Rothemund, N. Kellaris, C. Keplinger, How inhomogeneous zipping increases the force output of Peano-HASEL actuators. *Extreme Mech. Lett.* **31**, 100542 (2019).
74. A. Morton, "Lifetime of HASEL actuators," *Artimus Robotics*, 29 July 2021; www.artimusrobotics.com/post/lifetime-of-hasel-actuators.
75. I.-D. Sîrbu, D. Preninger, D. Danninger, L. Penkner, R. Schwödiauer, G. Moretti, N. Arnold, M. Fontana, M. Kaltenbrunner, Electrostatic actuators with constant force at low power loss using matched dielectrics. *Nat. Electron.* **6**, 888–899 (2023).
76. J. McMahon, S. K. Mitchell, K. Oguri, N. Kellaris, D. Kuettel, C. Keplinger, B. Bercovici, Area-of-effect softbots (AoES) for asteroid proximity operations, in *2019 IEEE Aerospace Conference* (IEEE, 2019), pp. 1–16.
77. T. Lodh, H. P. Le, Power electronic drivers for electrostatic HASEL actuators used in soft mobile robots. *IEEE J. Emerg. Sel. Top. Ind. Electron.* **5**, 994–1005 (2024).
78. R. Yang, M. Yang, P. Fan, T. Lu, T. Wang, A new flexible electrostatic generator using dielectric fluid. *J. Appl. Phys.* **134**, 105001 (2023).
79. N. Mendoza, B. Boren, J. Niffenegger, "Distributed embedded energy converter technologies for marine renewable energy: A technical report" (NREL/TP-5700-85158, Tech. Rep. National Renewable Energy Laboratory, 2023).
80. B. Boren, "Distributed embedded energy converter technologies (DEEC-Tec)" in *European Wave and Tidal Energy Conference* (NREL/CP-5700-80484, University of Southampton, 2023).
81. Z. Jiao, C. Zhang, W. Wang, M. Pan, H. Yang, J. Zou, Advanced artificial muscle for flexible material-based reconfigurable soft robots. *Adv. Sci.* **6**, 1901371 (2019).
82. S. A. Morin, Y. Shevchenko, J. Lessing, S. W. Kwok, R. F. Shepherd, A. A. Stokes, G. M. Whitesides, Using "click-e-bricks" to make 3D elastomeric structures. *Adv. Mater.* **26**, 5991–5999 (2014).
83. D. K. Patel, X. Huang, Y. Luo, M. Mungekar, M. K. Jawed, L. Yao, C. Majidi, Highly dynamic bistable soft actuator for reconfigurable multimodal soft robots. *Adv. Mater. Technol.* **8**, 2201259 (2023).

Acknowledgments: We thank the International Max Planck Research School for Intelligent Systems (IMPRS-IS) for supporting Z.Y. and I.S. We wish to also thank P. C. Johnsen for useful feedback, the Robotics Central Scientific Facility of the Max Planck Institute for Intelligent Systems (MPI-IS) for support with electronics and fabrication, A. Koh for helpful feedback regarding the model, and X. Li and X. Wang for reviewing the manuscript. **Funding:** This work was supported by the Max Planck Society, Germany (to Z.Y., E.H.R., I.S., and C.K.); the David and Lucile Packard Foundation (Z.Y., E.H.R., and C.K.); and the National Science Foundation Graduate Research Fellowship Program (NSF-GRFP; E.H.R.). **Author contributions:** Conceptualization: Z.Y., E.H.R., and C.K. Data curation: Z.Y., E.H.R., and I.S. Formal analysis: Z.Y. and E.H.R. Funding acquisition: E.H.R. and C.K. Investigation: Z.Y., E.H.R., I.S., and C.K. Methodology: Z.Y., E.H.R., I.S., P.R., and C.K. Project administration: Z.Y., E.H.R., I.S., and C.K. Resources: C.K. Software: Z.Y., E.H.R., and I.S. Supervision: C.K. Validation: Z.Y., E.H.R., and C.K. Visualization: Z.Y., E.H.R., I.S., and C.K. Writing—original draft: Z.Y. and E.H.R. Writing—review and editing: Z.Y., E.H.R., I.S., P.R., and C.K. **Competing interests:** C.K. is a coinventor on three patents, which cover the fundamentals and basic designs of HASEL actuators (assignee of all three patents is the Regents of the University of Colorado: US Patent 10995779B2, granted 2021-05-04; US Patent 11486421B2, granted 2022-11-01; and US Patent 11408452B2, granted 2022-08-09). C.K. is a cofounder of Artimus Robotics, a start-up company that commercializes HASEL actuators. The other authors declare that they have no competing interests. **Data and materials availability:** All data, code, and materials used in the analysis of this work can be found in the following repository: https://doi.org/10.17617/3.6HYXC4.

Submitted 5 January 2024
Accepted 20 August 2024
Published 18 September 2024
10.1126/scirobotics.adl3546

Downloaded from https://www.science.org at Max Planck Society on September 23, 2024